Isotropic and anisotropic surface wave cloaking techniques

OPEN ACCESS
IOP Publishing
Journal of Optics
J. Opt. **18** (2016) 044005 (9pp)
doi:10.1088/2040-8978/18/4/044005

Isotropic and anisotropic surface wave cloaking techniques

T M McManus, L La Spada and Y Hao

Antennas and Electromagnetics Research Lab, School of Electronic Engineering and Computer Science, Queen Mary, University of London, Mile End Road, London, E1 4NS, UK

E-mail: y.hao@qmul.ac.uk

Received 14 September 2015, revised 28 October 2015
Accepted for publication 30 October 2015
Published 1 April 2016

Abstract

In this paper we compare two different approaches for surface waves cloaking. The first technique is a unique application of Fermat's principle and requires isotropic material properties, but owing to its derivation is limited in its applicability. The second technique utilises a geometrical optics approximation for dealing with rays bound to a two dimensional surface and requires anisotropic material properties, though it can be used to cloak any smooth surface. We analytically derive the surface wave scattering behaviour for both cloak techniques when applied to a rotationally symmetric surface deformation. Furthermore, we simulate both using a commercially available full-wave electromagnetic solver and demonstrate a good level of agreement with their analytically derived solutions. Our analytical solutions and simulations provide a complete and concise overview of two different surface wave cloaking techniques.

Keywords: transformation optics, surface wave, invisibility cloak

(Some figures may appear in colour only in the online journal)

1. Introduction

Since the inception of transformation optics [1–4], many new and exciting devices have been proposed not only for electromagnetics space waves [5–13] ranging from cloaks to illusion devices, but also in the field of acoustics [14] and thermodynamics [15]. Over the past few years; however, there has been a growing interest in the manipulation of surface waves as well [16–29]. This particular study focuses on two methods of manipulating surface waves first proposed by Mitchell *et al* [16] and McManus *et al* [28], which are effectively an adaptation of Fermat's principle and a 2D approach similar to [1], respectively.

The importance of this work is that it is the first attempt, to the best of the authors knowledge, of a side-by-side comparison of two fundamentally, different surface wave cloaking schemes. In terms of practical importance, the manipulation of surface waves has applications in, but not limited to, communications (e.g. surface wave antennas) and obviously scattering reduction from undesirable, yet immovable surface deformations (SDs) (i.e. surface wave cloaking).

The overall structure of this article is as follows. First, we introduce the cloaking technique derived in [16], discuss some of its limitations and then solve for the required material overlay. Next, we derive a closed form analytical solution to show that said material overlay does in fact behave like a surface wave cloak. Then, we introduce the cloaking technique derived in [28], and follow the same procedure. Lastly, we use a commercially available full-wave electromagnetic solver (COMSOL 5.0) to further validate the performance of both methods and carry out a one-to-one comparison between them in terms of how well they emulate the amplitude, magnitude and phase of a surface wave travelling along a flat surface (i.e. how well they can be used as surface wave cloaks).

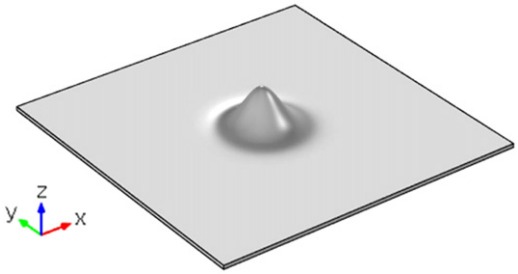

Figure 1. Isometric view of Gaussian surface deformation.

2. Two different cloaking techniques: theoretical approach

2.1. Isotropic cloaking formalism

Owing to the inherent limitations of the method proposed in [16], a rotationally symmetric SD is chosen as the test surface. Here a simple Gaussian deformation is selected due to its inherently smooth (no curvature mismatch between the flat approach-plane and the deformation itself) nature, something that was proven to be sought after in [16]. This surface is defined by

$$z = \sigma(x, y) = \mathrm{e}^{-\alpha\left(x^2+y^2\right)} \tag{1}$$

which can be recast in cylindrical coordinates as

$$z = \sigma(\rho, \theta) = \mathrm{e}^{-\alpha\rho^2}, \tag{2}$$

and is displayed in figure 1.

Setting out to determine the necessary material properties to cloak the SD from a surface wave leads to the following equations (3*a*) and (3*b*) where n_c is the cloaking refractive index that is sought, and $R(\phi)$ is the radial length from the centre of the origin to a point on the SD

$$n_c(\varphi)\sqrt{R(\varphi)^2 + R'(\varphi)^2}\,\mathrm{d}\varphi = \mathrm{d}r, \tag{3a}$$

$$2\pi R(\varphi)\sin(\varphi) n_c(\varphi) = 2\pi r, \tag{3b}$$

$$\frac{n'_c(\varphi)}{n_c(\varphi)} = \frac{\sqrt{R(\varphi)^2 + R'(\varphi)^2} - R'(\varphi)\sin(\varphi) - R(\varphi)\cos(\varphi)}{R(\varphi)\sin(\varphi)}. \tag{3c}$$

Here ϕ is as it is defined in polar coordinates. Utilising a simple finite difference approximation and setting $n_{c,1} = 1$, it is possible to solve for $n_c(\phi)$ numerically via

$$n_{c,i+1} = n_{c,i} - \Delta\varphi\left[\csc(\varphi_i) - \frac{R'(\varphi_i)}{R(\varphi_i)} + \cot(\varphi_i)\right]. \tag{4}$$

Equation (4) is solved and the resulting material profile (though for relative permittivity and not refractive index) is produced (see figure 2). Here it is important to note that this technique leads to an isotropic material overlay and in turn this cloak will be referred to as the isotropic surface wave cloak (ISC).

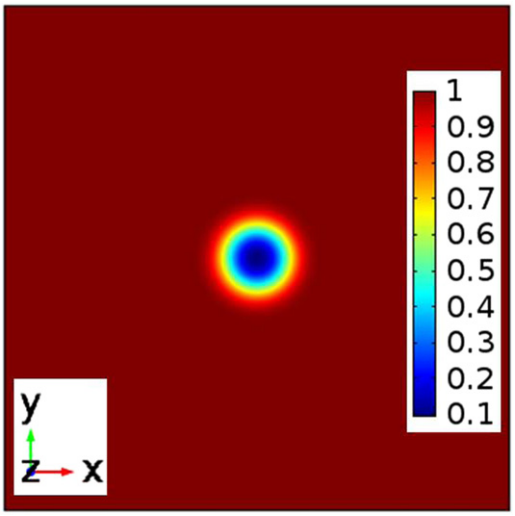

Figure 2. Isotropic ε_r profile as solved for by equation (4).

To describe the surface wave behaviour analytically, we start with the Helmholtz differential equation in two dimensional cylindrical form

$$\frac{1}{\rho}\frac{\partial}{\partial\rho}\left(\rho\frac{\partial E_z}{\partial\rho}\right) + \frac{1}{\rho^2}\frac{\partial^2 E_z}{\partial\theta^2} + kE_z = 0, \tag{5}$$

where by using separation of variables [30] we have

$$E(\rho, \theta) = R(\rho)\cdot\Theta(\theta). \tag{6}$$

Equation (5) is then recast as

$$\frac{\partial^2 R}{\partial\rho^2}\Theta + \frac{1}{\rho}\frac{\partial R}{\partial\rho}\Theta + \frac{1}{\rho^2}\frac{\partial^2\Theta}{\partial\theta^2}R + k^2 R\Theta = 0, \tag{7}$$

where upon multiplying both sides by $\frac{\rho^2}{R\Theta}$ results in

$$\left(\frac{\rho^2}{R}\frac{\mathrm{d}^2R(\rho)}{\mathrm{d}\rho^2} + \frac{\rho}{R}\frac{\mathrm{d}R(\rho)}{\mathrm{d}\rho} + \rho^2k^2\right) + \left(\frac{1}{\Theta}\frac{\mathrm{d}^2\Theta(\theta)}{\mathrm{d}\theta^2}\right) = 0. \tag{8}$$

The second part of equation (8) must be periodic implies that

$$\left(\frac{1}{\Theta}\frac{\mathrm{d}^2\Theta(\theta)}{\mathrm{d}\theta^2}\right) = -m^2, \tag{9}$$

meaning that it has solutions of the form

$$\Theta(\theta) = A_m\cos(m\theta) + B_m\sin(m\theta), \tag{10}$$

where A_m and B_m are constant coefficients, whose values depend on the chosen boundary conditions. Substituting equation (10) into (8) and using the following piece-wise defined permittivity distribution

$$\varepsilon(\rho) = \left(1 - \frac{a}{\rho^2}\right), \tag{11}$$

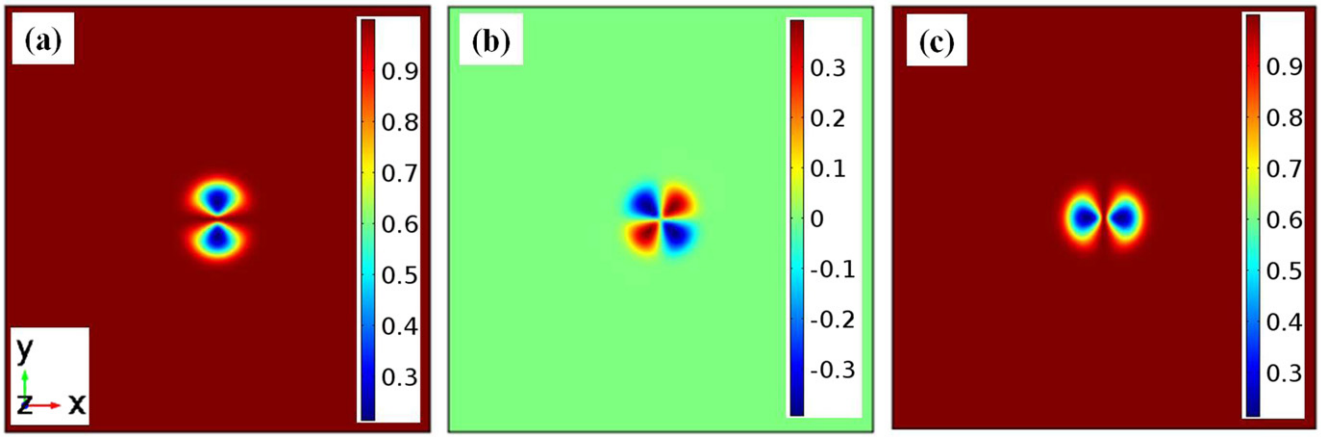

Figure 3. Anisotropic material properties called for by equation (18) where $\sigma = e^{-3(x^2+y^2)}$. (a) $\varepsilon_{xx} = \mu_{xx}$. (b) $\varepsilon_{xy} = \mu_{xy}$. (c) $\varepsilon_{yy} = \mu_{yy}$.

where the variable a is derived from the permittivity map found in figure 2, we obtain

$$\frac{\rho^2}{R}\frac{\mathrm{d}^2R(\rho)}{\mathrm{d}\rho^2} + \frac{\rho}{R}\frac{\mathrm{d}R(\rho)}{\mathrm{d}\rho} + \varepsilon(\rho)\rho^2k^2 = m^2, \tag{12}$$

which has solutions of the form

$$R(\rho) = C_mJ_A(k\rho) + D_mY_A(k\rho), \tag{13}$$

where $J_A(z)$ and $Y_A(z)$ are the Bessel function of the first and second kind, respectively, with $A = \sqrt{ak^2 + m^2}$.

Recombining the equations as proposed in equation (6) results in the desired solution

$$E(\rho, \theta) = \sum_{m=0}^{\infty}\Big[\big(A_m\cos(m\theta) + B_m\sin(m\theta)\big) \cdot \big(C_mJ_A(k\rho) + D_mY_A(k\rho)\big)\Big]. \tag{14}$$

2.2. Anisotropic cloaking formalism

In [28] the required material coating to cloak a SD is obtained as follows. To start, the E-field is written as an amplitude times a phase, $\mathbf{E} = \mathbf{a}e^{\mathrm{i}\mathbf{S}}$, and we assume that the phase of the wave varies (spatially) much more quickly than the amplitude of the wave, or the properties of the medium through which the wave is propagating. In doing so, Maxwell's equations can be recast as

$$\nabla\mathbf{S}\cdot\varepsilon\cdot\mathbf{a} = 0, \tag{15a}$$

$$\frac{1}{\omega}(\nabla\mathbf{S}\times\mathbf{a})e^{\mathrm{i}\mathbf{S}} = \mathbf{B}, \tag{15b}$$

$$\nabla\mathbf{S}\times\boldsymbol{\mu}^{-1}\cdot(\nabla\mathbf{S}\times\mathbf{a}) + \omega^2\varepsilon\cdot\mathbf{a} = 0. \tag{15c}$$

Then, assuming that the medium is in an electrically thin waveguide, the fundamental mode for the cavity is always normal to the top and bottom of the waveguide, meaning $\varepsilon_{zi} = \delta_{zz}$ and $\mathbf{a} = a\,\hat{\mathbf{z}}$. Then, equation (15$c$) is recast as

$$\frac{1}{|\tilde{\boldsymbol{\mu}}|}\left[\mu_{xx}\left(\frac{\partial S}{\partial x}\right)^2 + 2\frac{\partial S}{\partial x}\frac{\partial S}{\partial y}\mu_{xy} + \mu_{yy}\left(\frac{\partial S}{\partial y}\right)^2\right] = \omega^2, \tag{16a}$$

where

$$\boldsymbol{\mu} = \begin{bmatrix}\tilde{\boldsymbol{\mu}} & 0\\ 0 & 1\end{bmatrix}. \tag{16b}$$

Taking into consideration the eikonal equation in a general 2D coordinate system

$$\tilde{g}^{ab}\frac{\partial s}{\partial x^a}\frac{\partial s}{\partial x^b} = \omega^2, \tag{17}$$

we can relate equations (16a) and (17) to solve for the desired material parameters (see figure 3) to make a patch that is physically curved appeared to be electrically flat as detailed in [28] via

$$\varepsilon = \boldsymbol{\mu} = \frac{1}{1+(\nabla\sigma)^2}\begin{bmatrix}1+\left(\frac{\partial\sigma}{\partial x}\right)^2 & \frac{\partial\sigma}{\partial x}\frac{\partial\sigma}{\partial y} & 0\\ \frac{\partial\sigma}{\partial x}\frac{\partial\sigma}{\partial y} & 1+\left(\frac{\partial\sigma}{\partial y}\right)^2 & 0\\ 0 & 0 & 1+(\nabla\sigma)^2\end{bmatrix}. \tag{18}$$

Here it is important to note that any SD that can be defined parametrically (or more generally is a one-to-one mapping with a flat plane) can be cloaked using this method, and it is simply out of a desire to compare the ISC and ASC, that it is applied to a rotationally symmetric SD.

To demonstrate that the proposed solution is in fact valid for cloaking SDs from surface waves we start with one of the components of the solved for material tensor, ε_{xx}

$$\varepsilon_{xx} = \frac{1+\left(\frac{\partial\sigma}{\partial x}\right)^2}{1+(\nabla\sigma)^2} = \frac{e^{6\left(x^2+y^2\right)}+36x^2}{e^{6\left(x^2+y^2\right)}+36\left(x^2+y^2\right)}, \tag{19}$$

which can be can recast in cylindrical coordinates as

$$\varepsilon_{xx}(\rho, \theta) = \frac{e^{6\rho^2} + 36\rho^2 \cos^2(\theta)}{e^{6\rho^2} + 36\rho^2}. \tag{20}$$

Equation (20) is then separated into

$$\varepsilon_{xx}(\rho, \theta) = f(\rho) + \frac{g(\theta)}{\rho^2}, \tag{21}$$

where the radial and the angular functions can be expressed, respectively as:

$$f(\rho) = a\rho^2 + b \tag{22a}$$

and

$$g(\theta) = \cos(\theta). \tag{22b}$$

Following a similar procedure used for the ISC case, the Helmholtz differential equation is separable and takes on the form [30]:

$$\left(\frac{\rho^2}{R}\frac{\mathrm{d}^2R(\rho)}{\mathrm{d}\rho^2} + \frac{\rho}{R}\frac{\mathrm{d}R(\rho)}{\mathrm{d}\rho} + f(\rho)\rho^2k^2\right) + \left(\frac{1}{\Theta}\frac{\mathrm{d}^2\Theta(\theta)}{\mathrm{d}\theta^2} + g(\theta)\right) = 0. \tag{23}$$

This implies that the second part of equation (23) is

$$\left(\frac{1}{\Theta}\frac{\mathrm{d}^2\Theta(\theta)}{\mathrm{d}\theta^2} + \cos^2(\theta)\right) = -m^2, \tag{24}$$

which has solutions of the form

$$\Theta(\theta) = A_m C_a^q(\theta) + B_m S_a^q(\theta), \tag{25}$$

where C_a^q and S_a^q are the even and odd Mathieu functions, respectively, with characteristic values $a = m^2 + 1/2$ and $q = -1/4$. Focusing on to the radial components of equation (23), we have

$$\left(\frac{\rho^2}{R}\frac{\mathrm{d}^2R(\rho)}{\mathrm{d}\rho^2} + \frac{\rho}{R}\frac{\mathrm{d}R(\rho)}{\mathrm{d}\rho} + f(\rho)\rho^2k^2\right) = m^2, \tag{26}$$

which after some manipulation has a solution of the form

$$R(\rho) = e^{j\frac{\sqrt{a}}{2}kr^2}r^{1+m}\left(C_m U_A^B\left(C\cdot k\cdot\rho^2\right) + D_m L_{B-1}^{-A}\left(C\cdot k\cdot\rho^2\right)\right) \tag{27}$$

where $U_A^B(C\cdot k\cdot\rho)$ is the confluent hypergeometric function and $L_{B-1}^{-A}(C\cdot k\cdot\rho)$ is the generalised Laguerre polynomial, with $A = \frac{1}{4}\left(2 - j\frac{b}{\sqrt{a}}k + 2m\right)$, $B = 1 + m$, and $C = -j\sqrt{a}$. Recombining the component solutions solved for above, gives the general solution:

$$E(\rho, \theta) = \sum_{m=0}^{\infty}\Big[\left(A_m C_a^q(\theta) + B_m S_a^q(\theta)\right) \cdot \left(e^{j\frac{\sqrt{a}}{2}kr^2}r^{1+m}\left(C_m U_A^B\left(C\cdot k\cdot\rho^2\right) + D_m L_{B-1}^{-A}\left(C\cdot k\cdot\rho^2\right)\right)\right)\Big]. \tag{28}$$

3. Results and discussion

Utilising the same modelling technique proposed in [16, 27, 28, 31], where the behaviour of a surface wave is emulated by placing a medium in between two PEC sheets, and along the bounding edges, placing a perfectly matched layer, we model the devices. In all the following results, the method of excitation is a plane of unity amplitude polarized in the z-direction travelling from right to left. Also, it is important to keep in mind that the results displayed in figures 4–6 are for the total E-field which means it is a summation of both the incident and scattered fields.

Figure 4 displays E_z for a number of different surface configurations and angles of incidence: the SD is either uncloaked, cloaked with the isotropic material overlay (ISC) or cloaked with anisotropic material overlay (ASC).

Starting with figures 4(a) and (d) we note a large amount of forward surface wave scattering (FSWS) via the creation of mostly destructive interference patterns in the area behind the SD (sometimes referred to as the shadow region). Equally important to note is the very small amount of backward surface wave scattering caused by the uncloaked SD and this can be attributed to the smooth transition from the flat plane provided by equation (1) in figure 1.

Figures 4(b) and (e) displays the results for the ISC technique applied to the SD. Here it is clear that the cloak greatly reduces the amount of FSWS, but not entirely as one would expect considering that the formalism which it is based upon does not take into account magnitude preservation (it is only concerned with preserving electrical path lengths). The small amount of scattering that does occur in the forward direction, though difficult to see in figures 4(b) and (e) is easily identified in figures 5(b) and (e). Lastly, figures 4(c) and (f) demonstrates the ASC also greatly reduces the amount of FSWS, but is not entirely perfect in that a small amount of destructive interference is visible in its shadow region.

The reason for this is very similar to that of the ISC, in that the solution put forward in equation (18) is not concerned with mimicking the magnitude behaviour of a plane wave travelling along a flat surface, but instead its phase (eikonal equations). Ultimately, both of these techniques relay on the geometrical optics approximation and with that being said, one can also attribute the minor shadowing in the FSWS region to not ensuring that the devices are in fact electrically large.

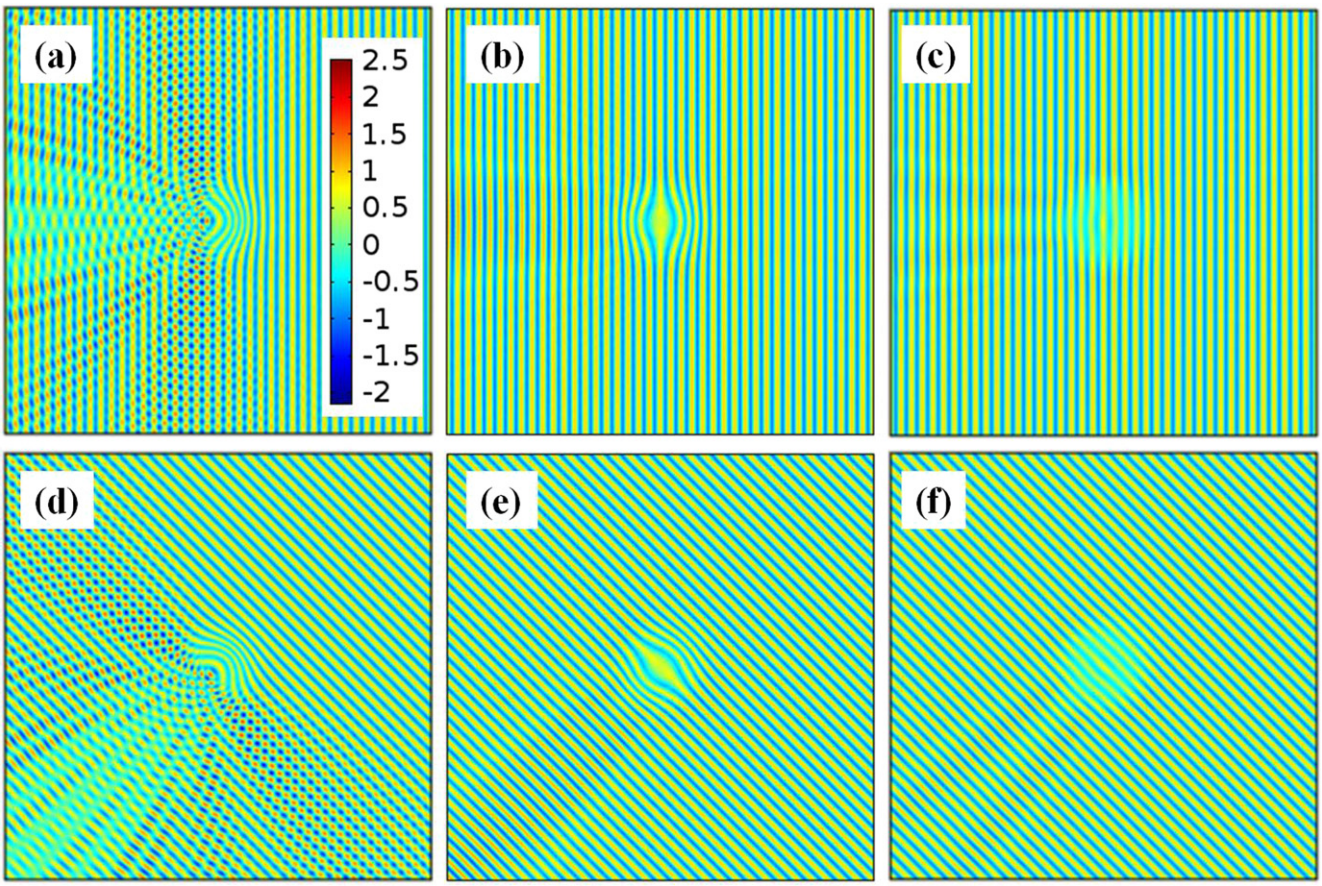

Figure 4. E_z for different surface configurations, and angles of incidence. (a) and (d) are for the uncloaked SD at $\theta_i = 0$ and $\pi/2$, respectively. (b) and (e) are for the ISC at $\theta_i = 0$ and $\pi/2$, respectively. (c) and (f) are for the ASC at $\theta_i = 0$ and $\pi/2$, respectively.

As E_z is effectively a function of both the magnitude and phase of E_z it makes sense to focus on these components in an attempt to gain a further understanding of how the ISC and ASC are behaving. In figure 5, $|E_z|$ is plotted for a number of different surface configurations and angles of incidence.

Starting with the uncloaked SD (figures 5(a) and (d)) the magnitude of the FSWS are far more pronounced (as they were alluded to figures 4(a) and (d)), and it is apparent that there are constructive interference patterns also established along the sides of the SD as well.

Figures 5(b) and (e) displays the results for the ISC where it is now apparent that a small amount of shadowing is in fact occurring. The same can be said for the ASC (figures 5(c) and (f)), but in this case there exists, in addition to the pattern seen in figures 5(b) and (e) a small 'beam' where the magnitude decreases. This 'beaming' effect is caused by the material gradient of the ASC not completely obeying the geometrical optics approximation mentioned earlier (the phase of the wave varies (spatially) much more quickly than the amplitude of the wave, or the properties of the medium through which the wave is propagating). To correct for this aberration, either the frequency of the incident wave would need to be increased or the decay rate (α in equation (1)) of the SD decreased.

Finally the phase behaviour for a number of different surface configurations and angles of incidence are displayed in figure 6. Starting with the uncloaked SD in figures 6(a) and (d) we note the extent to which the scattering is dictated by phase (as opposed to magnitude). Figures 6(b) and (e) displays the excellent phase preserving performance of the ISC, so much so in fact that if it were not for the SD itself in the centre of the plots, one would think it represented a surface wave travelling along a flat surface. Lastly, figures 6(c) and (f) demonstrates that the ASC performs just as well as the ISC in terms of phase-preservation and in this instance even the phase behaviour on the SD itself is virtually indistinguishable from the performance of surface wave travelling along a flat plane.

In an attempt to gain a deeper understanding of the FSWS behaviour of the ASC and ISC techniques a $10\lambda_0$ long probe line (see figure 7) is placed in the shadow region of the SD and the wave behaviour, as predicated by the numerical full-wave solution and the analytical solutions, is analysed.

Here we note the excellent level of agreement between the cloaks and a flat plane (first alluded to in figures 4–6) in terms of the amplitude (figure 8), magnitude (figure 9) and phase (figure 10) of E_z. Starting with figure 8, it can be seen that the ASC (red curve) virtually perfectly matches the spatial frequency and amplitude of the flat plane whereas the ISC (blue curve) is slightly out of phase and has greater amplitude variations relative to the flat plane. Next, inspecting the results for $|E_z|$ for the different cloaking techniques in

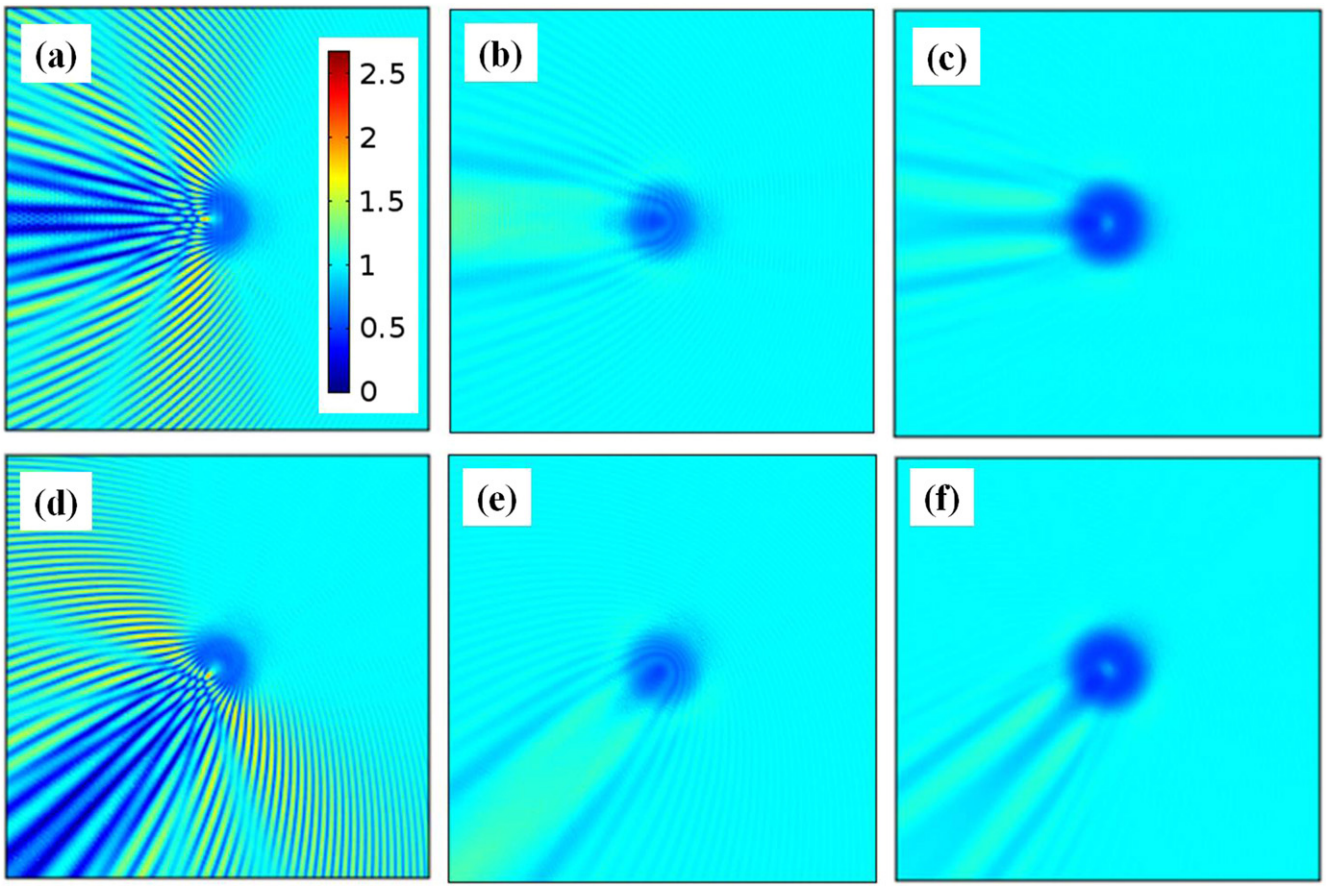

Figure 5. $|E_z|$ for different surface configurations, and angles of incidence. (a) and (d) are for the uncloaked SD at $\theta_i = 0$ and $\pi/2$, respectively. (b) and (e) are for the ISC at $\theta_i = 0$ and $\pi/2$, respectively. (c) and (f) are for the ASC at $\theta_i = 0$ and $\pi/2$, respectively.

figure 9, we note what a difference between the cloaked and flat configurations which, as mentioned previously, arises from an inherent limitation of the proposed cloaking techniques. Lastly, $\phi(E_z)$ along the probe line for the different cloaking techniques is plotted (see figure 10) and near perfect agreement is displayed by both cloaking techniques, but with the ISC results (blue curve) being slightly out of phase with the flat plane results (black curve).

To better understand the scattering loses from the two cloaks, an error study is conducted. First, a $20\lambda_0$ long probe line is oriented parallel to the incident plane wave ($\theta_i = 0$) at a distance of $10\lambda_0$ away from the centre of the SD on its exiting side (see inset of figure 11) and E_z is calculated for various surface configurations (see figure 11). In figure 11 it is demonstrated that both cloaking schemes slightly deviate from the ideal (flat surface) value of $1\,\mathrm{V\,m^{-1}}$ and this deviation can be regarded as one of the ways scattering loss can manifest itself. Note that E_z is not perfectly symmetric about the centre (at $10\lambda_0$) of the probe line because of a numerical artefact introduced by using the unstructured (and in turn often axially asymmetric) mesh used by the full-wave electromagnetic solver. In order to establish the level of agreement between the flat surface and the different cloaking techniques, the mean absolute error for each cloak is calculated. The mean absolute error (MAE) is defined as

$$\mathrm{MAE} = \frac{1}{n}\sum_{i=1}^{n}\left|E_{zf,i} - E_{zc,i}\right|, \tag{29}$$

where n is the number of points along the probe line and $E_{zf,i}$ and $E_{zc,i}$ are the field values for the flat surface and cloak respectively. Barring numerical artefacts, a perfectly functioning cloak would have a MAE of zero, meaning that there are no scattering loses. Using this metric, the cloak that has an MAE closer to zero would be considered the 'better' performing of the two and in this instance it is the ISC which has an MAE of 0.0361, which is slightly closer to zero than the MAE of the ASC which is 0.0376. To help put these values into context, the MAE for an uncloaked SD is 0.5320, which is 14.7315 and 14.1358 times greater than the MAE of the ISC and ASC, respectively.

Next, the scattering wave behaviour as predicted by equation (14) (ISC) and equation (28) (ASC) along the sample line in figure 7 is examined. Starting with figure 12 we note excellent levels of spatial frequency as well as amplitude agreement between the different surface configurations for analytically calculated values of E_z. In figure 13, the analytical results for calculating $|E_z|$ are displayed and the general trend of the ISC (blue curve) having a larger magnitude and the ASC (red curve) having a smaller magnitude (both

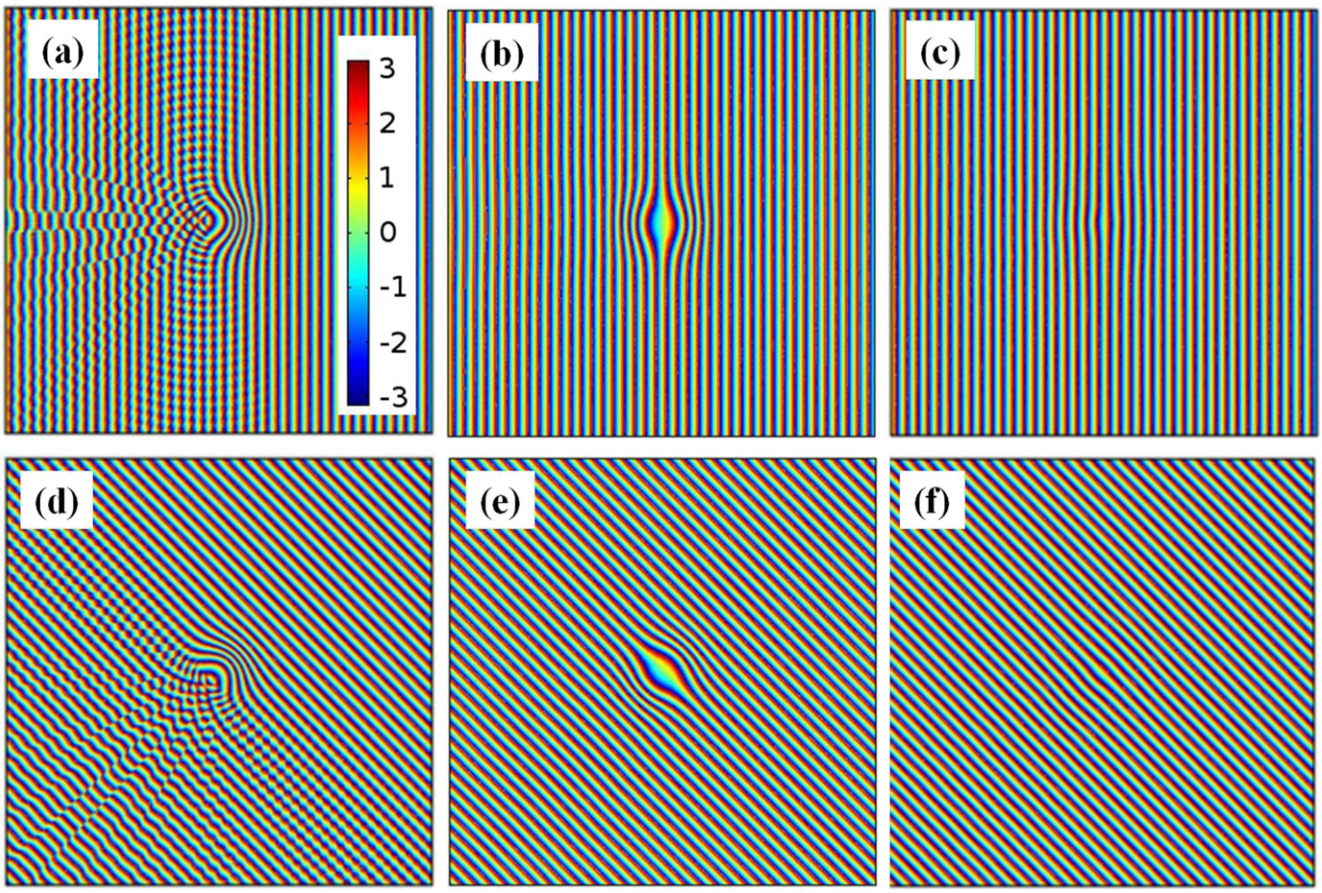

Figure 6. $\phi(E_z)$ for different surface configurations, and angles of incidence. (a) and (d) are for the uncloaked SD at $\theta_i = 0$ and $\pi/2$, respectively. (b) and (e) are for the ISC at $\theta_i = 0$ and $\pi/2$, respectively. (c) and (f) are for the ASC at $\theta_i = 0$ and $\pi/2$, respectively.

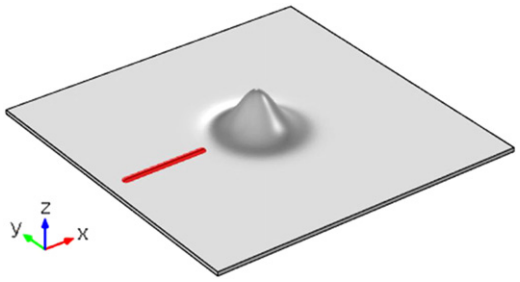

Figure 7. Isometric view of probe line in the shadow region of the SD.

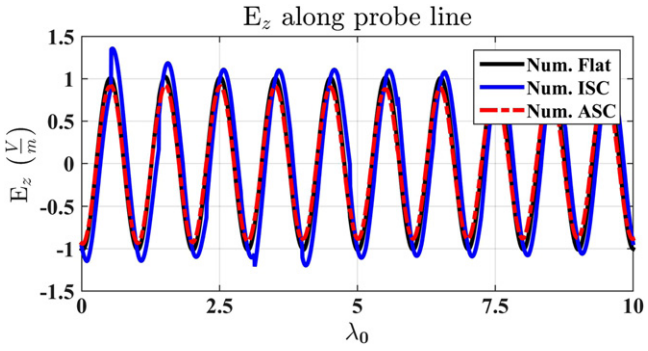

Figure 8. Numerically (COMSOL 5.0) determined E_z for different surface configurations for $\theta_i = 0$.

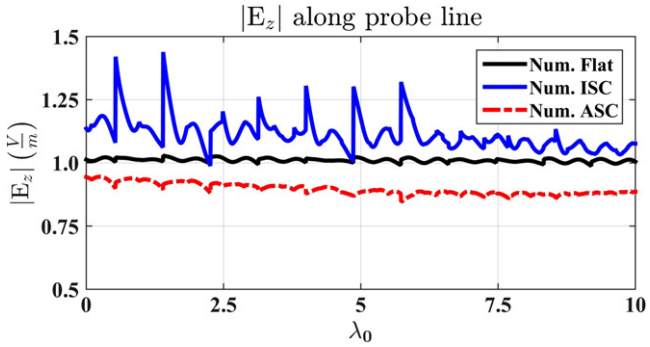

Figure 9. Numerically determined $|E_z|$ for different surface configurations for $\theta_i = 0$.

relative to the flat results represented by the black curve) is reproduced (see figure 8). However, the analytical and numerical results vary slightly here because the analytical solution only accounts for the fundamental order of the electric field function, whereas the numerical solution takes into account higher orders as well.

Lastly, inspecting the analytically determined phase behaviour for the different surface configurations (see figure 14), an exceptionally low level of disagreement is demonstrated with the ISC (blue curve) and ASC (red curve) nearly perfectly emulating the flat surface phase behaviour

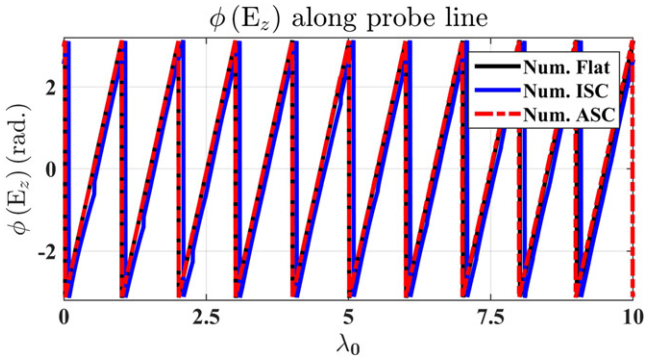

Figure 10. Numerically determined $\phi(E_z)$ for different surface configurations for $\theta_i = 0$.

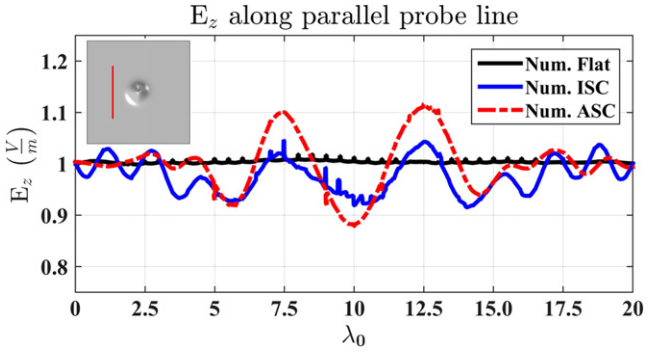

Figure 11. Numerically determined E_z for different surface configurations for $\theta_i = 0$, along a probe line oriented parallel to an incident field.

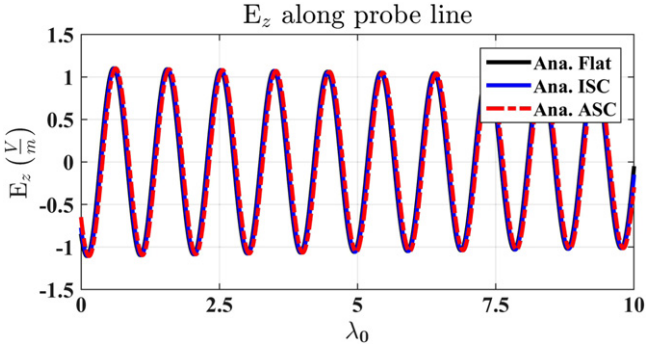

Figure 12. Analytically determined E_z for different surface configurations for $\theta_i = 0$.

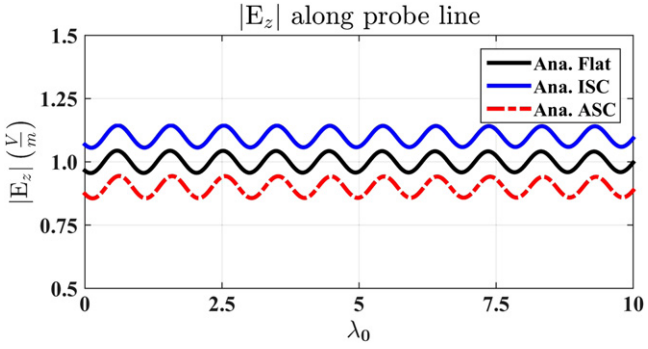

Figure 13. Analytically determined $|E_z|$ for different surface configurations for $\theta_i = 0$.

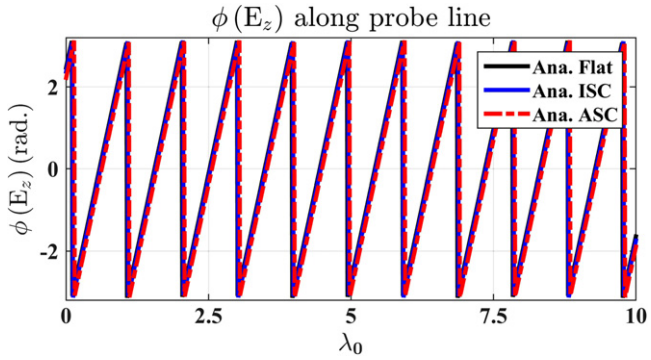

Figure 14. Analytically determined $\phi(E_z)$ for different surface configurations for $\theta_i = 0$.

(black curve). Thus, after analysing the full-wave simulation results (figures 4–6) and the numerical/analytical quantitative study (figures 8–14) one can conclude that both techniques offer exceptional, though slightly differing (depending upon the field parameter of interest), levels of performance.

4. Conclusions

In this paper, two different surface wave cloaking techniques were compared. The first was borne out of a unique application of Fermat's principle and allowed for the creation of an isotropic material overlay though the cloaked SD itself had to be rotationally symmetric. An analytical solution to Helmholtz's equation in two dimensions was derived with the SDs material coating included, and it was demonstrated that it emulated the behaviour of a surface wave travelling along a flat plane (i.e. performed as a cloak).

The second technique that was investigated was an adaptation of a formalism previously used for structures in three dimensions. This method was a truly generalised one in the sense that it could deal with any SDs as long as it was able to be parameterized by two variables. In turn this meant it could deal with surfaces that the first technique could not immediately handle, but for the sake of comparison with the ISC its usage was limited to a rotationally symmetric SD. Once the necessary material properties for the cloak were determined it was shown analytically (via solving Helmhotz's equations in two dimensions) that once again, the proposed material overlay did in fact behave as a surface wave cloak.

Lastly it is demonstrated, via a number of full-wave electromagnetic simulations, (COMSOL 5.0) that both cloaks offered an excellent level of performance (phase-front preservation) for multiple angles of incidence, and multiple measurements (i.e. amplitude, magnitude and phase). This statement is further supported by a quantitative study involving the analysis of the wave behaviour along a sample line in the shadow region of the SDs (as solved for by both the numerical and analytical solutions). A scattering loss study is also included that quantifies just how well the proposed cloaking schemes perform relative to both an ideal perfectly cloaked SD as well as uncloaked SD.

Acknowledgements

This work was funded by the Engineering and Physical Sciences Research Council (EPSRC), UK under a Programme Grant (EP/I034548/1) 'The Quest for Ultimate Electromagnetics using Spatial Transformations (QUEST)'.

References

[1] Leonhardt U 2006 Optical conformal mapping *Science* **312** 1777
[2] Leohhardt U and Philbin T G 2006 General relativity in electrical engineering *New J. Phys.* **8** 247
[3] Leonhardt U and Philbin T G 2010 *Geometry and Light: The Science of Invisibility* (New York: Dover)
[4] Pendry J B, Schurig D and Smith D R 2006 Controlling electromagnetic fields *Science* **312** 1780
[5] Schurig D *et al* 2006 Metamaterial electromagnetic cloak at microwave frequencies *Science* **314** 977
[6] Leonhardt U and Tyc T 2008 Broadband invisibility cloaking by non-euclidean cloaking *Sci. Express* **323** 110
[7] Cai W, Chettiar U K, Kildishev A V and Shalaev V M 2007 Optical cloaking with metamaterials *Nat. Photonics* **1** 224–7
[8] Li J and Pendry J B 2008 Hiding under the carpet: a new strategy for cloaking *Phys. Rev. Lett.* **101** 203901
[9] Lai Y, Chen H, Zhang Z and Chan C T 2009 Complementary media invisibility cloak that cloaks objects at a distance outside of the cloaking shell *Phys. Rev. Lett.* **102** 093901
[10] Chen T and Yu S R 2010 Design of optical cloaks and illusion devices along a circumferential direction in curvilinear *J. Appl. Phys.* **108** 093106
[11] Patel A M and Grbic A 2014 Transformation electromagnetics devices based on printed-circuit tensor impedance surfaces *IEEE Trans. Microw. Theory Tech.* **62** 1102–11
[12] Gok G and Grbic A 2010 Tensor transformation-line metamaterials *IEEE Trans. Antennas Propag.* **58** 1559–66
[13] Argyropoulos C, Kallos E and Hao Y 2011 Bandwidth evaluation of dispersive transformation electromagnetics based devices *Appl. Phys.* A **103** 715–9
[14] Farhat M, Enoch S, Guenneau S and Movchan A B 2008 Broadband cylindrical acoustic cloak for linear surface waves in a fluid *Phys. Rev. Lett.* **101** 134501
[15] Guenneau S, Amra C and Veynante D 2012 Transformation thermodynamics: cloaking and concentrating heat flux *Opt. Express* **20** 8207–18
[16] Mitchell-Thomas R C, McManus T M, Quevedo-Teruel O, Horsley S A R and Hao Y 2013 Perfect surface wave cloaks *Phys. Rev. Lett.* **111** 213901
[17] Quarfoth R and Sievenpiper D 2014 Surface wave scattering reduction using beam shifters *IEEE Antennas Wirel. Propag. Lett.* **13** 963–6
[18] Kim S and Sievenpiper D 2014 Theoretical limitations for TM surface wave attenuation by lossy coatings on conductive surfaces *IEEE Trans. Antennas Propag.* **62** 475–80
[19] Zedler M and Eleftheriades G V 2011 Anisotropic transmission-line metamaterials for 2D transformation optics applications *Proc. IEEE* **99** 1634–45
[20] Huidobro P A, Nesterov M L, Martin-Moreno L and Garcia-Vidal F J 2010 Transformation optics for plasmonics *Nano Lett.* **10** 1985
[21] Huidobro P A, Nesterov M L, Martin-Moreno L and Garcia-Vidal F J 2011 Moulding the flow of surface plasmons using conformal and quasiconformal mappings *New J. Phys.* **13** 033011
[22] Kadic M, Guenneau A and Enoch S 2010 Transformational plasmonics: cloak, concentrator and rotator for SPPs *Opt. Express* **18** 12027–32
[23] Kadic M, Dupont G, Guenneau S and Enoch S 2011 Controlling surface plasmon polaritons in transformed coordinates *J. Mod. Opt.* **58** 994–1003
[24] Yang R and Hao Y 2012 An accurate control of the surface wave using transformation optics *Opt. Express* **20** 9341–50
[25] Baumeier B, Leskova T A and Maradudin A A 2009 Cloaking from surface plasmon polaritons by a circular array of point scatterers *Phys. Rev. Lett.* **103** 246803
[26] Elser J and Podolskiy V A 2008 Scattering-free plasomonic optics with anisotropic metamaterials *Phys. Rev. Lett.* **100** 066402
[27] Mitchell-Thomas R C, Quevedo-Teruel O, McManus T M, Horsley S A R and Hao Y 2014 Lenses on curved surfaces *Opt. Lett.* **39** 3551–4
[28] McManus T M, Valiente-Kroon J A, Horsley S A R and Hao Y 2014 Illusions and cloaks for surface waves *Sci. Rep.* **4** 5997
[29] Xu S, Xu H, Gao H, Jiang Y, Yu F, Joannopoulos J D, Soljacic M, Chen H, Sun H and Zhang B 2015 Broadband surface-wave transformation cloak *PNAS* **12** 7635–8
[30] Moon P and Spencer D E 1988 *Field Theory Handbook, Including Coordinate Systems, Differential Equations, and Their Solutions* 2nd edn (New York: Springer)
[31] Walter C H 1960 Surface-wave luneberg lens antennas *IRE Trans. Antennas Propag.* **8** 508